

**16. Electrocatalysis on surfaces modified by metal monolayers
deposited at underpotentials**

Radoslav Addzic
Brookhaven National Laboratory
Upton, NY 11973-5000

Chapter submitted to:
Encyclopedia of Electrochemistry
A. Bard and M. Stratmann, Editors
Vol. 1, Wiley-VCH Publishers

17. Electrocatalysis on surfaces modified by metal monolayers deposited at underpotentials

Radoslav Addzic
Brookhaven National Laboratory
Upton, NY 11973-5000

16.1 Introduction

The remarkable catalytic properties of electrode surfaces modified by monolayer amounts of metal adatoms obtained by underpotential deposition (UPD) have been the subject of a large number of studies during the last couple of decades. This interest stems from the possibility of implementing strictly surface modifications of electrocatalysts in an elegant, well-controlled way, and these bi-metallic surfaces can serve as models for the design of new catalysts. In addition, some of these systems may have potential for practical applications. The UPD of metals, which in general involves the deposition of up to a monolayer of metal on a foreign substrate at potentials positive to the reversible thermodynamic potential, facilitates this type of surface modification, which can be performed repeatedly by potential control. Recent studies of these surfaces and their catalytic properties by new *in situ* surface structure sensitive techniques have greatly improved the understanding of these systems.

In the mid seventies, it was demonstrated that UPD metal adatoms can produce electrocatalytic effects on various electrochemical reactions. These include oxidation of small organic molecules, oxygen reduction, reactions of electroorganic synthesis, electrodeposition of metals, and charge transfers in redox couples. The oxidation of organic molecules that are potential fuels for fuel cells attracted special attention. In the

electrodeposition of metals, in addition to causing catalytic effects, the UPD metal adlayers can cause dramatic improvement in the morphology of the deposits. Inhibition is also often observed, in particular for H₂ evolution and hydration of hydride-forming metals by the adlayers of metals with high hydrogen evolution overpotentials. Two reviews exist on the work prior to 1984 [1] and 1985 [2].

In this review, after a brief overview of the structural and electronic properties of metal adlayers, there are six sections describing catalytic effects on redox couples, oxidation of organic molecules, carbon monoxide, organic electrosynthesis reactions, hydrogen evolution, oxygen reduction and metal electrodeposition. Outside the scope of this review are other UPD processes that play a role in determining the catalytic properties of electrode surfaces such as the UPD of H and OH.

16.2 Structural and electronic properties of electrode surfaces with metal adlayers

Structural and electronic properties of electrode surfaces covered by foreign metal adlayers (usually with submonolayer coverage) are expected to be considerably different from either those of the substrate or the adsorbate bulk metals. The structure of the top surface layer will be that of the adlayer, determined by the substrate surface structure, adatom size and coverage, substrate-adsorbate interaction and in some systems, by interaction with coadsorbed anions (See Chapter 14 in this Volume). Major advances in the understanding of metal adlayer structural behavior have been achieved by recent applications of *in situ* scanning probes [3] and surface x-ray scattering techniques [4]. In general, for high coverage metal adlayer phases which form at potentials close to the

reversible potentials of bulk deposition, incommensurate, hexagonal or quasihexagonal structures are common. The interatomic distances are potential-dependent, often having values below the distances in bulk materials. This phenomenon has been termed electrocompression. Commensurate adlayer structures are less common and usually form with coadsorbed anions.

The structural studies with single crystal surfaces have clarified to a large extent the questions of electrosorption valences and partial charge of metal adatoms at large adatom coverages. Close to the reversible deposition potential, the adatoms are neutral species; otherwise, the electrocompression would not be observed. In low-coverage phases, electrosorption valences below unity may be expected, with the charge on the adatoms usually compensated by the coadsorbed anions.

The work function of the metal surface is considerably altered by the adsorption of foreign atoms. This is well established at the metal/vacuum interface. Pb adlayers on Ag cause a pronounced decrease in the work function with increasing Pb coverage [5]. A similar change can be expected at the electrode surface. The potential of zero charge (PZC) of the electrode surface, which is directly related to the work function, has been determined for the Pb adlayer on polycrystalline Ag. A value close to that was found for bulk Pb [6].

Optical properties of metal adlayers were extensively studied in the late seventies by reflectance spectroscopy, ellipsometry, surface plasmon excitation, and Mössbauer spectroscopy (See ref. 1 and 2 and references therein). Pronounced changes of reflectivity are caused by the UPD adlayers, in particular on substrates that exhibit large electroreflectance signals, *viz.*, Au, Ag, and Cu. The optical properties of submonolayers

and monolayers of metals were found to be markedly different from the properties of bulk phases. New insights into electronic properties of these systems have been obtained by application of synchrotron radiation-based x-ray absorption techniques (XAS). The x-ray absorption near-edge structure spectroscopy (XANES) measurements of Pb on Pt show that in the underpotential deposition region the Pb species are essentially neutral Pb atoms [7]. Fig. 16.1 shows the effect of changes in potential on the normalized Pb XANES. The XANES indicate the presence of neutral species at all potentials except at 1.15V where Pb is desorbed and the spectra indicate the presence of Pb^{2+} . There was no evidence of Pb interaction with oxygenated species in the UPD region.

The electronic properties of a monolayer of Pb [8] and Tl [9] on Ag(111) electrode surfaces have been calculated by using a density functional formalism. Calculations show that, as for metal surfaces in general, the excess charge in the electronic density profile lies in front of the metal surface. The work function of the Tl monolayer on Ag(111) was found to be close the bulk Tl value [9]. For a Pb monolayer, calculations predict almost the same interfacial capacity as for a surface of Pb(111). The latter result is in accord with the experimental data for polycrystalline Ag [6].

16.3 Electrocatalysis on surfaces modified with metal adlayers

16.3.1 Redox reactions

The effects of the UPD adlayers on the rates of electrode reactions were first investigated for the $\text{Fe}^{2+}/\text{Fe}^{3+}$ and $\text{Ti}^{3+}/\text{Ti}^{4+}$ redox reactions on Au, which were found to be slightly increased by adlayers of several metals [10]. The energy levels involved in the

redox reactions are those of the adsorbates, not of the substrates, and these systems seemed ideal to provide insights into the unresolved question of the role of the nature of the metal electrode in the kinetics of the outer-sphere redox reaction. The charge transfer in these “non-catalytic” reactions takes place in the outer Helmholtz plane. Consequently, it should not be significantly affected by the metal adlayer. The data reported so far are in accord with this statement (cf. references [1] and [2]), thus confirming a small role that the nature of the metal electrode has these reactions. In a recent work, Nagy et al. [11] took special care to remove traces of chlorides that can be coadsorbed with metal adatoms and that can increase the concentration of cations in the double layer. This effect could account for the small increase of the redox reactions by metal adlayers. Even in the absence of trace amounts of chloride, small enhancements in the $\text{Fe}^{2+}/\text{Fe}^{3+}$ reaction rates caused by Bi on Pt and Ag on Au were found. No effect was observed for a Cu adlayer on the reaction on Au. Rhodes et al. [12] found an enhanced rate of a $\text{Cr}^{3+}/\text{Cr}^{2+}$ reaction in HCl on Au by Bi, Pb, Tl and Sn adlayers, and attributed this to the enhanced adsorption of Cl^- in the presence of adatoms. Chlorides make bridges that are necessary for this complex, inner-sphere, redox couple reaction to occur.

Several mechanisms have been proposed to explain the small enhancement effects of metal adatoms. A change in PZC caused by metal adlayers should induce a change in the ϕ_2 potential and thus affect the rate of redox couples. The calculations of the ϕ_2 potential in 1M H_2SO_4 solution using PZC for bulk Bi showed that the effect is too small to explain the observed rate increase [13]. The density of electronic states at the Fermi level was considered by Adami and Despi [10] and analyzed in detail by Schmickler [14]. He suggested that the difference between the adsorbate density of states at the

solvent configuration corresponding to the saddlepoint of the reaction hypersurface and the density of states of the metal electrode could explain the catalytic effects. The expression for the current was derived in terms of the adsorbate density of states. Nagy et al. [11] reported electronic structure calculations using the extended H_{ckel} molecular-orbital method to determine whether the magnitude of the electronic coupling in the presence of adlayers can cause catalytic effects. For the reaction at the Cu adlayer on Au, the calculation shows that the ion can approach 0.04 +/- 0.02 nm closer to the Cu/Au surface than to the bare Au surface. This can increase the electronic factor by 2-14 times, thus increasing electronic coupling and the reaction rate, although the nature of the electronic coupling remains unchanged. Iwasita et al. [15] found no effect of Pb and Tl adatoms on Pt on the rate of a very fast Ru(NH₃)₆²⁺/Ru(NH₃)₆³⁺ couple. Fonseca et al. [16] measured the effects of Pb, Bi and Cd on the rates of Fe²⁺/Fe³⁺, Fe(CN)₆⁴⁻/Fe(CN)₆³⁻ and IrCl₆³⁻/IrCl₆²⁻ redox reactions, and confirmed small enhancements of the rates of these redox couples.

In contrast to the simple redox reactions, the rates of the redox processes involving organic couples are considerably increased by metal adlayers on electrode surfaces. Some examples include quinhydrone, pyrocatechol/o-benzoquinone, adrenaline/adrenalinquinone, and other quinone-type redox couples [2]. Fig. 16.2 shows data obtained for the pyrocatechol/o-benzoquinone system on Pt/Bi_{ad}. A considerable increase in reversibility caused by metal adlayers has been attributed by Kokkinidis [17] to the change of the reaction mechanism, from an “inner-sphere” mechanism on a Pt surface with adsorbed intermediates, to an “outer sphere” reaction on Pt/M_{ad} surfaces

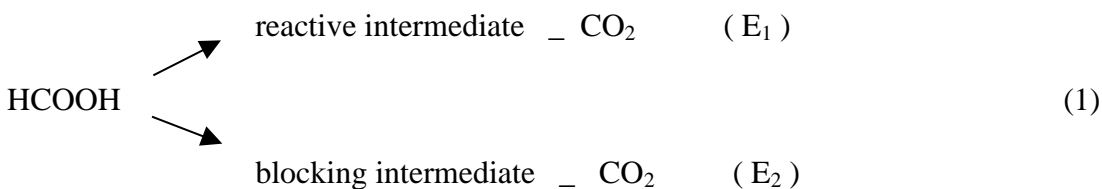
without adsorbed intermediates. Fonseca et al. [16] confirmed large effects of of Pb, Bi and Cd on the rates of several types of hydroquinone/quinone couples.

16.3.2 Oxidation of organic molecules

16.3.2.1 Formic Acid

Catalytic effects of various magnitudes, some quite striking, are caused by monolayers of Pb, Bi, Tl, Cd, Sn, Sb, Se and Ge on the oxidation of organic molecules that are potential fuels for fuel cells *viz.*, HCOOH, CH₃OH, HCHO, CH₃CHO, CO, glucose and other monosaccharides, ethylene glycol and some aliphatic alcohols on Pt, as well as on some other platinum metals (see reviews of previous work in references [1,2]. Slow rates are characteristic of the oxidation of these organic molecules even with the best catalysts because of the generation of strongly bonded intermediates - poisoning species - that reduce their activity. Upon adsorption, dehydrogenation and subsequent oxidation of adsorbed hydrogen are fast reactions that leave strongly bonded fragments on the surface. Their oxidations require very positive potentials that are impractical for fuel cells applications. The UPD metal adatoms can reduce the poisoning effects by several mechanisms (*vide infra*), thus causing the catalytic effects.

There is a consensus regarding the mechanism of the oxidation of formic acid on Pt which involves a dual path mechanism [18] with direct oxidation to CO₂, and an indirect mechanism through a blocking intermediate:



where $E_2 > E_1$. An indication for the dual path mechanism is provided by isotope-labeling experiments of Heitbaum et al. [19, 20]. Strong evidence for the reactive intermediate branch comes from infrared spectroscopy data showing generation of CO_2 at potentials where CO is not oxidized [21]. On the basis of a kinetic isotope effect for the oxidation of HCOOH and DCOOH on Pt(111) and Pt(100), it was concluded that the rate determining step is H-C bond scission [22].

The nature of the strongly bound intermediate in the oxidation of formic acid, methanol, and formaldehyde has been a long-disputed issue. CO appears to be the principal poisoning adsorbate, while other adsorbates, such as COH and CHO, are difficult to detect. These species appear less stable than CO and may be slow-reacting intermediates [23]. In the oxidation of HCOOH on Pt, COH and/or CHO were proposed as poisoning species on the basis of coulometric determination of a number of electrons per site (e.p.s.) used for the oxidation of adsorbate [18], differential electrochemical mass spectrometry (DEMS) [19], and radiotracer measurements [24]. Bewick and coworkers [25] employed electrochemically modulated IR spectroscopy (EMIRS), which clearly identified CO as the poisoning species. This was strongly supported by further work [26]. Two e.p.s. were found for several single crystal surfaces which also suggest that CO is a poison [23,27]. More details on this topic can be found in reviews in references [28,29,30].

The mechanism of the catalytic action of metal adlayers in the oxidation of organic molecules has been interpreted by using several models including a “third body” effect, an electronic effect, and the bifunctional catalyst mechanism.

- (i) Third-body effect

A third-body effect, which is equivalent to an “ensemble” effect in heterogeneous catalysis, is based on the role of metal adatoms in blocking the surface sites for a side reaction that generates poisoning species, or in blocking the adsorption of the inhibiting species, which requires more than one surface site for adsorption. The reaction in the main pathway can proceed at the unoccupied sites that now form smaller ensembles. In this model, adatoms do not enhance the rate on the uncovered substrate sites. In electrocatalysis, the effect was proposed by Conway et al. [31] to interpret the effect of acetonitrile on formic acid oxidation on Pt. The third body effect is operative for any adsorbate statistically distributed on the surface that is not desorbed upon adsorption of reacting species and intermediates of reactions.

ii) Bifunctional mechanism

The bifunctional mechanism, often used in catalysis, has been considered in electrocatalysis by Cathro [32] and Shibata and Motto [33]. The surface is considered to have two types of sites that have distinct roles in the reaction. The substrate, such as Pt, breaks the bonds in organic molecules upon adsorption, while the adatom can adsorb oxygen-containing species that can oxidize strongly adsorbed intermediates such as CO. Oxygen adsorption on adatoms is expected to occur at potentials negative of oxygen adsorption on Pt. This facilitates CO oxidation at potentials more negative than on bare Pt, thus freeing the surface for the main reaction.

iii) Electronic effects

Electronic effects can result from the modifications of the properties of uncovered near-neighbor sites and next near-neighbor sites. The adatoms modified in the interaction with substrates, may, *per se*, take part in reactions.

Striking catalytic effects observed in the oxidation of formic acid on Pt modified by Pb and Bi adlayers are shown in Fig. 16.3 [34]. Currents in anodic sweeps are enhanced by almost two orders of magnitude, which is also observed in steady state measurements [34,35,36]. Fig. 16.4 shows quasi-stationary curves for the Pb/Pt system as a function of Pb coverage[†]. For the optimum coverage of $\theta_{\text{Pb}} = 0.73(0.36)$ the enhancement is about three orders of magnitude as calculated per Pb-free Pt surface. Similar effects were observed with Tl adlayers [34, 37, 38], but the effects of Cd are considerably smaller [34]. Cd was partially desorbed by HCOOH and reaction intermediates, while the Pb coverage was unaffected, as determined by reflectance spectroscopy measurements [39]. In accordance with this observation, IR measurements show no effect of Cd on CO adsorbate on Rh in HCOOH oxidation, while Pb decreased the coverage of the bridge-bonded CO [23]. Catalytic effects were observed with other platinum metals *viz.* Rh, Pd and Ir [40]. Smaller enhancements were observed than with Pt, the smallest being observed with Pd [41], which is the least poisoned Pt-metal. The catalytic effects of less common UPD systems such as Se, Ge, As and Te [42,43], Hg [37], Ag and Cu [1] on Pt have also been reported and are smaller than those observed with Pb and Bi.

The results of the studies with single crystal electrodes [44,45,46,47,48] have demonstrated the existence of a structural dependence of the magnitude of the catalytic effects. The role of the adlayer structure in determining the observed dependence has not

[†] Metal adatom coverages are defined in two ways throughout the literature reviewed in this text. According to one definition, the coverage is defined as the ratio between the number of covered and total number of substrate atoms. The coverage is also defined as a number of atoms of adsorbate per one atom of substrate. The latter definition is becoming used more often. For large adatoms, the difference in the coverage values from the two definitions can be very large. In order to simplify comparison of results, and to preserve the link to original work when the coverages are given according to the first definition, approximate coverages calculated by using the second approach are appended in parentheses.

been clearly determined so far. In most studies, the adlayer structures were derived from coverages obtained from voltammetry. It is, however, necessary to determine adlayer structures during the course of HCOOH oxidation because of the sensitivity of adatom ordering to the interaction with other adsorbates. For instance, *in situ* x-ray scattering techniques show that the ordered (3 x 3) Pb adlayer on Pt(111) vanishes during HCOOH oxidation, but the Pb coverage remains unaffected [49]. Further work is needed to determine whether the adlayer structure has an influence on the magnitude of the catalytic effect, or whether only the adatom coverage is important.

An extension of the UPD modification of the electrocatalytic properties of electrode surfaces is a process described as an “irreversible” adsorption of metal adatoms on electrode surfaces. These adsorbates can be obtained by adsorption from cation-containing solution without the application of external potential. Janssen and Moolhuyzen [50] demonstrated that immersion of clean Pt surfaces in solution containing metal salts, and subsequent emersion and removal of the excess solution, could produce adlayers of metal adatoms. Clavilier and coworkers [46] used this procedure with several metal adsorbates on Pt single crystal electrodes. These “preadsorbed” layers are quite stable. It is, however, necessary to control the electrode potential, since the adlayer coverage is potential independent only within certain potential limits. In some cases, as for Bi on Pt, it is believed that the adsorbate changes oxidation states with potential and that therefore both species interact with a surface forming adlayer [51]. *Ex situ* XPS data show that the charge should be attributed to OH⁻ adsorption rather than to a change in the valence state of adsorbed Bi [52].

There is no satisfactory description of the “irreversible” adsorption process. It was ascribed to chemical reaction with adsorbed hydrogen [50], and to a local cell mechanism through PtOH formation [53]. The interaction of cations with the surface M-OH species should also be considered as a possible mechanism, since it is known that they can strongly interact with oxidized surfaces [54,55]. This was observed even at very positive potentials, as in the case of the oxide monolayers on Au and Pt [56]. Except for Bi, generally small catalytic effects of the preadsorbed adatoms on Pt single crystal electrodes were reported usually at positive potentials for Sb [57], As [58], Sn [59], Se [60] and Te [61]. An analysis of metal adlayers causing the most interesting effects is presented below.

Lead Pronounced effects of Pb (Fig. 16.3) were interpreted in terms of a third-body effect by Adami et al. [34]. Pb adatoms suppress adsorption of hydrogen and strongly bound intermediates, in particular those interacting with two or three surface sites. The same model was assumed for Bi and Tl. Adsorbed H was considered to take part in the formation of strongly bound intermediates [18]. Current responses to potential sweeps into the H adsorption region [18,62], and crystal quartz microbalance measurements [63] provide evidence for fast poison accumulation in the presence of H_{ads} . An analysis of the rates for Pb modified Pt showed that, for adatoms covering evenly θ of the sites, there are no multi-bonded poisoning species adsorbed [40]. In agreement with the experiment, the model predicted the maximum activity at $\theta_M = 0.5(0.25)$. Pletcher and Solis [35] also found maximum activity at $\theta_M = 0.5(0.25)$. Shibata et al. [43] found evidence that the adatom size determines the effect which increases with the number of occupied sites. The most pronounced effect was found for Bi, the largest adatom. Pb caused the largest

effects according to the data in references [34,35]. Xia and Iwasita [64] used DEMS combined with the ^{13}C labeling to make a distinction between CO_2 formed from bulk solution and from adsorbed species (Fig. 16.5). ^{12}C -formic acid oxidation was observed in the presence of a known Pb coverage and the adsorbate from ^{13}C -formic acid. Pb catalyzes the HCOOH oxidation from bulk solution on a bare Pt surface, and also helps in the oxidation of HCOOH adsorbates. The HCOOH oxidation could not take place for Pt completely covered by Pb and HCOOH adsorbates. The electronic interaction of Pb and Pt was assumed to take place in order to explain the catalytic effects. The maximum catalytic effect was found at $\theta_{\text{Pb}} = 0.5(0.25)$ for oxidation potentials $>250\text{mV}$, and $\theta_{\text{Pb}} = 0.8(0.4)$ for potentials $<250\text{mV}$. At $\theta_{\text{Pb}} = 0.84(0.42)$, no adsorbate formation is possible, but the oxidation of bulk acid still takes place. The increased activity of the remaining bare Pt has been interpreted by reaction of HCOOH with H_2O modified in the interaction with Pt-Pb sites [65]. This activity is still lower than the intrinsic activity of Pt(100) determined by pulsed voltammetry [66]. Kita and coworkers [48] reported almost the same magnitude for the catalytic effects of UPD Pb and preadsorbed Pb on Pt(111). The maximum effect was observed for a Pb coverage of 0.29, which almost completely prevented the adsorption of CO. These authors also indicate that a third body effect and a bifunctional mechanism cannot fully explain the observed effects. To summarize, for Pb, a part of the observed catalytic effect is due to a third body effect, but there is a growing evidence for the electronic effect to be partly responsible for the catalysis.

Bismuth Large effects of Bi have been found in several studies [34,43]. Clavilier et al. [46] showed that Bi preadsorbed on Pt(111) enhances the kinetics of HCOOH oxidation in a large interval of coverages from 0 to 0.8(0.27) at potentials below 0.6V. The

accumulation of strongly bound intermediates is suppressed at very small Bi coverages. This suggests that the next-nearest neighbors Pt atoms must be affected by Bi and that the third body effect cannot account for the inhibition of the poison formation. At high Bi coverages, large currents are measured at potentials where Bi adsorbs OH [52]. Therefore, in that potential region, it could act through the bifunctional mechanism. Fig. 16.6 shows voltammetry curves for Pt(111) with $\theta_{\text{Bi}}=0.82(0.27)$ and the oxidation of HCOOH on that surface [46]. Weaver and coworkers [67] reported an IR study of this system which shows small CO coverages on Pt(111), even in the absence of Bi. This surface is the least poisoned surface from the low-index planes. The optimal coverage of Bi was 0.2, which was interpreted in terms of an ensemble, *i.e.*, a third body effect. An enhancement factor of approximately two orders of magnitude is cited in both works [46,67], and is similar to that observed with the UPD Bi adlayer [34].

Two roles were assumed for Bi on Pt(100) [46]. First, Bi inhibits formation of poison through a third body type effect. The poison coverage decreases linearly and becomes zero at $\theta_{\text{Bi}}=0.45(0.22)$. Second, the highest HCOOH oxidation rates are observed at high Bi coverage, $\sim \theta_{\text{Bi}}=0.9(0.45)$, which indicates a direct role of Bi in the oxidation of HCOOH, that is, an electronic effect is operative in this system. The maximum rate is, however, still lower than the intrinsic rate on Pt(100). Bi forms on Pt(100) a $c(2 \times 2)$ adlayer with a coverage of $\theta_{\text{Bi}}=0.5$, with adatoms residing at bridge positions [68]. Therefore, at $\sim \theta_{\text{Bi}}=0.45$, a small number of Pt sites apparently remains uncovered and a direct participation of Bi in the reaction appears likely. Weaver and coworkers [67] showed by infrared spectroscopy a complete cessation of CO formation at $\theta_{\text{Bi}} = 0.2$, which is in good agreement with ref [46]. The catalytic effect of Bi was

ascribed to the attenuation of the degree of CO poison formation on Pt(100), which the authors interpreted in terms of a third body effect.

Recent work involved stepped Pt surfaces with controlled adsorption of Bi on step edges [69]. For the stepped single crystal surfaces Pt(554), Pt(332) and Pt(221), with nine-, five- and three-atom wide terraces, respectively, the enhancement factor for HCOOH oxidation increases as the terrace width decreases. Bi appears to block adsorption of poison on reactive (110) oriented step sites and decreases the reaction ensemble size, which increases the rate on narrow (111) terraces.

Leiva et al. [70] reported the simulation of the catalytic effects of several adatoms by using the model in which both adatoms and poisoning species block one surface site. Eight and six near neighbors covered by adatoms protect one site from poison adsorption on square and hexagonal lattices, respectively. The adatoms are assumed to be adsorbed randomly at 50 x 50 lattices up to the coverage of θ_M , and then the poison is adsorbed up to θ_P . The oxidation currents are calculated for such a configuration for several catalytic cases. In the Pt(111)/Bi system, Bi-Pt pairs were assumed to be responsible for the catalytic effect, without poison formation. Fig. 16.7 shows a comparison between the experiment and the calculated curve. The agreement is surprisingly good considering the incorrect assumptions that adatoms cover one surface site and that they are randomly distributed. Bi is known to inhibit three H adsorption sites on Pt(111) [71]. Nevertheless, the simulation data seem to corroborate the electronic effect for the Bi/Pt system. The data for Pt(111) and Pt(100) revealed the role of substrate in determining the effect of Bi in suppressing poison adsorption (the electronic effect for Pt(111), but a third body for Pt(100)). In addition, on the same surface (Pt(100)), Bi can suppress poison formation by

a third body effect, and can catalyze the oxidation of HCOOH through an electronic effect.

Antimony The effect of Sb adlayers on Pt(100) [57] were ascribed to the suppression of poison formation, and the maximum oxidation current is obtained at high coverage, $\theta_{\text{Sb}} = 0.9(0.3)$, when no poison is detected at the surface. Substantial currents are observed for this surface. The maximum activity, however, does not surpass the intrinsic activity of Pt(100). A third body effect was found operative for this system.

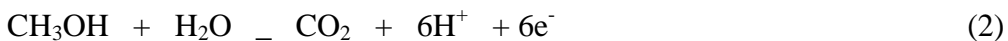
Kizhakevariam and Weaver [72] found that Sb inhibits the adsorption of CO on Pt (100) and Pt (111) by decreasing the two-fold binding geometries deduced from the relative ν_{CO} band intensities. The optimum catalysis for Pt(100) is observed at $\theta_{\text{Sb}} = 0.35$. Sb causes significant up-shifting of the CO band formed from HCOOH oxidation, which suggests that dissociative chemisorption is triggered at adjacent sites, electronically modified by Sb. Fig. 16.8 shows IR spectra for Pt(100) and Pt(100) with an Sb adlayer ($\theta_{\text{Sb}}=0.25$) and the corresponding oxidation current vs. θ_{Sb} and θ_{CO} curves. The enhancement has been interpreted in line with third body and electronic effects [72]. Good agreement was found between the simulated effects and experimental data for the Sb/Pt(100) system where Sb was assumed to obey the third body effect [70].

Noble metal monolayers The systems involving a deposition of ultra thin layers of noble metals on noble metal substrates, such as Ru on Pt [73,], or Pd on Pt [74] or on Au [75], exhibit enhancements of the oxidation of organic molecules. These systems are outside the scope of this review, and will be only mentioned here. In general, deposition of such layers occurs at overpotentials, and they, unlike the UPD adlayers, cannot be dissolved except at extreme positive potentials. Usually, such deposition produces 2D or 3D

clusters, but pseudomorphic deposits can also be formed, as in the case of Pd on Au(111) [76,77], and Pt on Au(111) [78]. Ru can be “spontaneously” deposited in an electroless process on Pt [79]. Ru layers catalyze oxidation of methanol on Pt [79], and Pd enhances the oxidation of HCOOH on Au [75] and Pt [80] single crystal electrodes. The activity of the Pd-modified surfaces depended markedly on the Pd layer thickness and on their crystallographic orientation.

16.3.2.2 Oxidation of methanol

Methanol is considered the most attractive fuel for fuel cells and its reaction has been thoroughly investigated on surfaces modified by metal adatoms. The overall reaction involves the exchange of six electrons per molecule:



This is a multistep reaction, which probably proceeds through a sequential dehydrogenation that can produce several intermediates, as indicated in the general scheme proposed by Bagotzky et al. [81]. Details of the dehydrogenation of methanol on Pt have not been established. From kinetic isotope measurements of CD₃OH and CH₃OH oxidation, it was shown that the first removal of H in the reaction



is the rate-determining step [82,83].

For methanol, more than for formic acid, evidence points out that besides CO there is at least one additional adsorbate - the COH species. Three e.p.s. values are found often for adsorbate oxidation and show that it has to contain a H atom [84]. Beden et al. [85] reported from IR measurements the linear, bridge bonded CO and CHO-like species

or species with a carbonyl bond. By using subtractively normalized Fourier transform infrared spectroscopy (SNFTIRS), Iwasita et al. [86] have determined absolute absorption bands for linear-, bridge-, multi-bonded CO and COH adsorbates. Nichols and Bewick [87], by using a flow IR-electrochemical cell, identified COH and CH_xOH species as reactive intermediates. Recent results with DEMS indicate predominantly a mixture of CO and COH, or only CO as adsorbed intermediates [84,88, 89]. Model calculations of methanol oxidation on Pt(111) that provide a good fit to the experimental data without adjustable parameters involve a reactive intermediate with the stoichiometry H:C:O [90].

Negligible catalytic [2,91,92], and predominantly inhibition effects [93] are observed for methanol oxidation on Pt in acid solutions. The exceptions are the effects of Sn [50, 94,95], and Ge [95]. Significant catalytic effects have been observed for Pb, and Bi on Pt in alkaline solutions [96,97]. However, carbonization of the alkaline electrolyte with CO_2 makes these systems unsuitable for practical applications. For single crystal Pt(100) and Pt(111) surfaces, the reaction has been found to be inhibited by the Bi adlayer [47,98].

Some agreement exists on the effects of Sn, although the results are not reproducible. The UPD of tin differs from the majority of the UPD systems [99]. Its oxidation state is extremely potential dependent. The effects of Sn on the oxidation of CH_3OH on Pt are attractive because they occur at very low potentials. The system Pt-Sn has been investigated in three forms: Sn irreversibly adsorbed, Sn adsorbed by UPD, and ordered single crystal Pt_3Sn alloy [100]. Vassiliev et al. [94] found a Temkin adsorption behavior of neutral Sn at Pt in the potential region from 0 V to 0.2. Above 0.2 V tin undergoes a partial oxidation to Sn^+ , or SnOH at $\sim 0.5\text{V}$. A ten-fold increase of the rate in

the presence of Sn has been found and has been ascribed to the bifunctional mechanism [91]. Frelink et al. [101] demonstrated by ellipsometry that a submonolayer of Sn-oxide disappears from Pt surfaces in the presence of methanol. The reports of considerable catalytic effects of Sn [50,95] have not been reproduced in recent studies [23,102,98]. Inhibition was observed for the methanol oxidation on Pt(111) and Pt(100) with Sn adlayers [98], and for Pt₃Sn alloys [100]. Janssen and Moolhuysen [50] concluded that Pt is modified through a ligand, that is through an electronic effect, while Motoo and coworkers [103] proposed that a bifunctional mechanism is operative for Sn. Bittins-Cattaneo and Iwasita [102] found that Sn(II) species are responsible for the catalytic effect, which can form a hydroxy-complex like Sn(OH)⁺ that can transfer O to the organic residue. The activity was ascribed to a suitably oriented adsorbed H₂O on a Pt/Sn surface. Fig. 16.9 shows a linear sweep voltammetry and mass signal of CO₂ for Pt and Pt with adsorbed Sn. The observed enhancement of methanol oxidation is in the middle range of those reported so far. Molecular orbital studies demonstrated that Sn atoms on Pt(111) can weaken CO adsorption [104], but subsequent work showed that Sn in the Pt surface does not attract H₂O or activate the formation of the OH_{ads} species that can oxidize CO intermediates [105]. The data on Sn indicate that its state on Pt surfaces is highly dependent on surface structure and on the method of Sn deposition, which determine its catalytic properties for CH₃OH oxidation. Catalytic effects are often observed with dispersed Pt, while inhibition is usually observed with flat surfaces. While the potential for practical application of Sn modified Pt for methanol oxidation is small, this system provides a strong support for the importance of bifunctional catalysts for methanol oxidation.

16.3.2.3 Carbon Monoxide

Carbon monoxide is a model adsorbate for studying molecular adsorption in catalysis and electrocatalysis. It is a major poisoning species in the oxidation of small organic molecules, which is an additional motivation for studying its oxidation. The reaction on metal adlayer covered surfaces can reveal information useful for the design of new electrocatalysts for the oxidation of methanol and reformat hydrogen. Metal adlayers affect the adsorption behavior of CO and can cause small enhancements of its oxidation. CO interacts so strongly with Pt that it can displace many metal adlayers. Lukas et al. [68] demonstrated by SXS studies that CO causes displacement of Cu and Pb adatoms from Pt(100) and Pt(111) surfaces, while a $c(2 \times 2)$ -Bi structure on Pt(100) is unaffected by CO in solution phase. Motoo and coworkers have reported pronounced effects of Sn and Ge [95], and As [106] on the oxidation of dissolved CO on Pt. Sn causes a shift of CO oxidation on Pt by 400mV to more negative potentials. This effect was explained in terms of the bifunctional catalyst. The same mechanism was proposed for the effects of Pb, As, Sb, and Bi [107], although there is no evidence for oxygen coadsorption with Pb, while a weak evidence was reported for other three metals.

Preadsorbed Bi adatoms were found to preferentially block CO adsorption at bridge sites, and at saturation Bi coverage, $\theta_{Bi} = 0.2$, only linear CO is observed on Pt(111) [108]. Bi causes a decrease of CO oxidation [109] on Pt(100), which agrees with its stabilization of this adsorbate deduced from *in situ* IR studies [110,111], while As has an opposite effect [111]. Both adatoms modify the CO stripping process with a small

catalytic effect observed at very positive potentials (0.7V). The catalysis has been ascribed to the adatom-mediated oxygen transfer with a possible electronic effect for As [111]. Similar behavior is observed with Sb, which decreases the adsorption of CO on Pt(100) and Pt(111) surfaces by removing the two-fold bridging geometry, as deduced from the relative ν_{CO} band intensities [72]. At the saturation Sb coverage only linear CO is observed.

Baltruschat and coworkers [112] reported a large negative shift of CO oxidation to 0.25V caused by Sn adsorbed at step sites on Pt (332) and Pt(755) stepped surfaces (Fig. 16.10). Sn adsorbs preferentially at the step sites, which can be deduced from the inhibition of H adsorption on the step sites from voltammetry curves [113]. The effect has been ascribed to a destabilization of the CO molecules due to repulsion between CO and Sn. This repulsion shifts the CO molecules into a so-called “high coverage” state, which can be oxidized at low potentials as shown for Pt-Sn alloy surfaces [114]. (This state is not formed in oxidation of methanol on this alloy, which was offered as an explanation of the inhibition effect observed in that reaction.) The CO oxidation rates at low potentials are, however, very sluggish. The effect of Sn on the reaction on Pt(111) was found to be negligible. The activity of stepped Pt surfaces is certainly related to the observed effect of Sn on polycrystalline Pt [91], which usually has a high density of steps.

16.3.2.4 Other organic molecules

In addition to the oxidation of formic acid and methanol, the oxidation of a considerable number of organic molecules is catalyzed by metal adlayers on Pt [1,2].

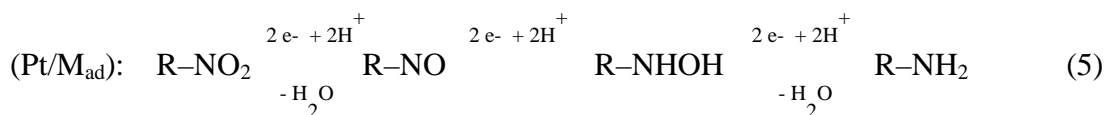
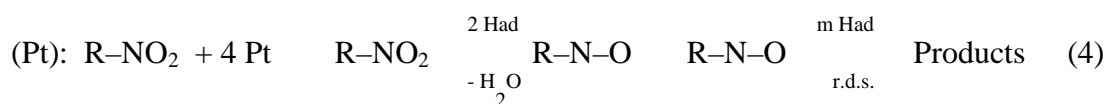
These include formaldehyde [115], various aliphatic alcohols including ethyl, propyl and butyl alcohols, ethylene glycol and glycerol [97], propane-diol [116,117,118], ascorbic acid [119], glucose and other monosacharides [2,120], propane [121] and lactonic acid [122]. Some of the observed effects are very large, as seen in the oxidation of HCHO on platinum metals [1,115]. In general, the effects observed seem to be caused by reduction of adsorption of strongly bonded intermediates. Large inhibition was observed for the oxidation of hydrazine on Pt (2). The reactions of highly oxygenated molecules such as squaric, croconic, rhodizonic acids and tetrahydroxy-p-benzoquinone on Pt were also found to be affected by metal adlayers. Bi and Se were found to promote the cleavage of these molecules on Pt(111) by the third body effect.

16.3.3 Electroorganic synthesis

Electroorganic synthetic reactions on surfaces modified by metal adlayers have not received as much attention as the oxidation of small organic molecules, although it is quite conceivable that this type of surface modification can have interesting catalytic effects and can affect the selectivity of various synthetic pathways. In addition to the elimination of poisoning effects from chemisorbed organic fragments, another useful effect of metal adatoms is an increased potential window in which the electrode materials such as Pt can be used for such reactions. At potentials where the modified electrodes can be used, the electrodes of metals undergoing the UPD, such as of Pb, Bi or Tl are not stable. Most of the work in this area was done by Kokkinidis and coworkers [2] who demonstrated catalytic effects of metal adlayers for the reduction of nitro and nitroso compounds [123,124], and for the catalytic hydrogenation of some unsaturated

hydrocarbons [2]. While the reduction of the nitro group is catalyzed by metal adlayers on Pt, the reduction of nitrobenzene is partially inhibited on Ag by Pb adatoms [125]. A number of publications exist in the Russian literature about the effect of cation addition on various electroorganic synthetic reactions that are not discussed in terms of the UPD effects, although most of the systems probably involve the metal adlayer formation (see references in [1]).

Electroreduction of nitro-compounds is of considerable importance for electroorganic synthesis. Interesting catalytic effects were reported for the reduction of aromatic nitro compounds on Pt. Fig. 16.11 shows that Pb, Tl and Bi adlayers shift the half-wave potential positively by 100-300 mV. The catalytic effect was attributed to a change in the mechanism of the reduction of the nitro-group from a catalytic hydrogenation on bare Pt, to an electron transfer mechanism on Pt/M_{ad}, *i.e.* a direct electron exchange between the nitro compound and the adatom-covered electrode surface, *viz.*,



The same change from the “catalytic” to the “electron transfer” mechanism has been observed in benzofuroxan reduction on Pt with several metal adlayers [2].

The reduction of heterocyclic nitro compounds on platinum is also considerably catalyzed by metal adlayers. The reaction of 3-nitro-1H-1,2,4-triazole on Pt/M_{ad} is a four-electron reduction also involving the electron transfer mechanism, while the hydrogenation occurs on bare Pt [126]. This activity surpasses that of mercury electrodes in alkaline solutions. The reaction on Au follows an electrocatalytic and/or electron exchange mechanism. The electrocatalytic mechanism gives a diffusion-controlled cleavage of the N-O bond, while the electron exchange mechanism proceeds through dihydroxylamine, which can react further. On Au/M_{ad}, the reduction proceeds through dihydroxylamine [127]. Selective oxidation of lactose to lactobionic acid on Pt/Pb_{ads} with a significant enhancement of the reaction rate in comparison with the one on Pt has been reported by Druliolle et al. [128].

Motoo and Furuya [129] demonstrated an enhancement of the ethylene reduction on Pt by Cu and Ag and inhibition by Se and Tl adlayers. Cu and Ag adatoms, which block one Pt site, desorb the ethylene molecule which blocks 2.5 Pt sites, thus leaving 1.5 sites available for H adsorption. Hydrogen adatoms at these sites facilitate a higher rate of ethylene reduction. Tl and Se adatoms cause inhibition since they block 2.5 sites as ethylene does.

16.3.4 Hydrogen evolution

Hydrogen evolution has been found without exception to be inhibited by adlayers of Bi, As, Cu and Sn, on Pt [130, 131], Pb, Tl and Cd on Pt [132] and Au [132], and by Pb and Tl on Ag [133] electrodes. All these metals exhibit a large overpotential for hydrogen evolution. Adlayers inhibiting H₂ evolution are of interest for fundamental

electrocatalysis and electrode kinetics, but they also have practical significance in promoting sorption of H into some metals, altering selectivity for some hydrogenation reactions, and in corrosion inhibition. The lattermost is possible when O₂ reduction is not enhanced by metal adlayers.

The observed inhibition on Pt has been ascribed to [132]: i) simple geometric blocking, ii) a decrease in the number of pairs of uncovered Pt atoms, which decreases the H + H recombination reaction, and (iii) a change of electronic states of uncovered Pt atoms. Protopopoff and Marcus [134] have analyzed in detail the blocking effects of sulfur on H₂ evolution on Pt(110) and Pt(111) electrodes. For random adatoms distribution, the zones of deactivation overlap, and this process can be analyzed by using a simple statistical treatment [135]. For several Pt/M_{ad} systems, considerable H₂ evolution takes place when the UPD of H is completely blocked. This provides an additional proof that there is no connection between the UPD H and the intermediates in H₂ evolution.

The UPD metal adlayers have interesting effects on the reaction mechanism. Pb, Tl and Cd at small coverages cause pronounced inhibition, but the Tafel slope for the reaction remains -30mV, as for bare Pt. This means that the recombination of two H atoms giving H₂ (H_{ad} + H_{ad} → H₂) is the rate determining step for both surfaces. At larger Pb coverages, the Tafel slopes becomes -120 mV (Fig. 16.12) because there are no pairs of Pt atoms for a recombination reaction to occur, and the mechanism with the ion-plus-atom reaction (H_{ad} + H⁺ + e⁻ → H₂) rate-determining step becomes operative [132]. Changes of slope from -30 to -60 and -120 mV have been reported for Pt with Ge [131]. No change of Tafel slope was found for H₂ evolution on Au/Pb [132] since on bare Au the ion-plus-atom reaction is the rate-determining step requiring one surface site.

Inhibition of H₂ evolution was reported for stationary single crystal electrodes for As/Pt(111) [136], Bi/Pt(100), Sb/Pt(100), Bi/Pt(111) and Sb/Pt(111) [137] surfaces. For the Bi/Pt(111) system, the polarization curves have slopes of -30 to -35 mV for $\theta_{\text{Bi}} < 0.04$ (0.02), and for $0.14(0.07) < \theta_{\text{Bi}} < 0.33(0.18)$, the slopes are -35 and -54 mV at small and high overpotentials, respectively [137] (Fig. 16.13). For Pt(100), a linear decrease of the H₂ evolution current as a function of coverage has been observed up to $\theta_{\text{Bi}} = 0.35(0.18)$, and a steep decrease has been observed above it. For Pt(111), a large decrease of H₂ evolution was observed at small Bi coverages up to 0.1(0.03), and a linear decrease was seen for larger coverages. A similar observation was made for polycrystalline Pt with Pb [132]. Small changes of Tafel slope for low Bi coverages were explained by a hypothetical mechanism in which a slow recombination and an ion-plus-atom reaction rate determining steps occur in parallel. Inhibition effects of As, which is a prototype catalytic poison, have been reported for polycrystalline electrodes [138,139] and for a Pt(111) surface [136]. Surprisingly small inhibition was observed up to $\theta_{\text{As}} = 1/3(1/6)$ for the latter system.

The mechanism of significant H₂ evolution on Pt with large coverage of inhibiting metal adatoms is not clear. For Bi on Pt(100), the existence of the c(2 x 2) Bi adlayer was assumed, and it was proposed that H₂ evolution takes place through four-fold symmetry holes in the adlayer [137]. This adlayer exists at Pt(100) [68], but its structure still needs to be verified during H₂ evolution. *In situ* verification of the adlayer structure during the course of H₂ evolution has been obtained by SXS for Pt(111) with a Tl adlayer [140]. Fig. 15 shows data for Tl adlayers on Pt(111) in solutions of two different pH values. A significant H₂ evolution current flows at Pt(111) despite the close packed configuration of

the Tl adlayer. The electrocompression of the Tl-Tl distance with decreasing potential is observed with this system. H₂ evolution has no effect on the structure of the Tl adlayer, but the Tl-Tl distance ceases to contract at its onset (Fig. 16.14). It is likely that in addition to defect sites, H₂ evolution occurs through hollow sites in the structure of the Tl adlayer. This prevents further compression with decreasing potential. These data seem to corroborate the assumption for the H₂ evolution through the hollow sites in the Bi adlayer on Pt(100).

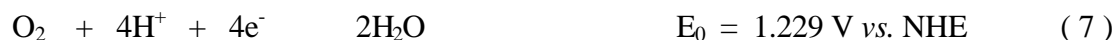
Several approaches were used to quantify inhibition effects of metal adlayers. These involved calculations of currents of H₂ evolution based on the order-disorder theory of alloys [130,132], and simulations based on geometric [137,139], and long-range electronic effects [137]. Verification of the models used in some simulations seems necessary in order to obtain a more complete understanding of the inhibition effects.

Related to the inhibition of H₂ evolution is the effect cations on the corrosion of iron. Dra_i_ and Vorkapi_ [141] interpreted a decrease of the corrosion of Fe in sulfuric acid in the presence of Mn²⁺, Cd²⁺ and Zn²⁺ in terms of the inhibition of H₂ evolution by the UPD of these metals. Similar effects were observed for Pb, Tl [142,143] and for Ge, Ga [144]. In deaerated solutions, the inhibition effect can be quite pronounced. In the presence of O₂, however, an enhanced O₂ reduction can increase corrosion rates.

16.3.5 Oxygen reduction

Oxygen reduction is a multielectron reaction that involves several elementary steps in the reaction mechanisms. In aqueous solutions, oxygen reduction appears to occur by two over-all pathways: a "direct" four-electron reduction, and a "peroxide"

pathway that involves H_2O_2 as the intermediate [145]. For acid solutions, the reaction in a direct four-electron pathway is:



Two electrons are exchanged in a “peroxide” pathway:



Peroxide can undergo further reduction,



or it can catalytically decompose into O_2 and H_2O . Peroxide is the final reduction product on some less active surfaces. On some surfaces, the two pathways can occur in parallel. The same pathways are operative in alkaline solutions but at different set of potentials involving intermediates and products determined by the solution pH [145].

16.3.5.1 Alkaline solutions

Foreign metal adatoms cause remarkable catalytic effects on oxygen reduction on several electrode surfaces. The adatoms of Pb [146, 147], Bi [148], and Tl [149,150] cause a shift of the half-wave potential of the O_2 reduction to more positive values and an approximate doubling of the diffusion limited current density. The latter is due to the change of the reaction mechanism from a two-electron reduction on Au into a vital four-electron reduction on Au covered with UPD metal adlayers. Catalytic effects were observed also for Pt [151], glassy carbon and graphite [2], and Ru [152] surfaces with Pb and Tl adsorbates. The latter three cases are somewhat different from the UPD adlayers on metal surfaces. For carbons, it appears that the UPD occurs through an interaction of metal with carbon surface groups. For oxidized Ru surfaces, cations interact with surface oxides.

Fig. 16.15 shows rotating disk-ring measurements of O₂ reduction on Au and Au/Pbad. The upper panel shows the UPD of Pb on Au in NaOH solution. The disk current shows doubling of the diffusion limited current, which means that four electrons are exchanged in the reaction on Pb/Au. Consequently, the ring current shows that peroxide generation is almost completely suppressed. A series reaction mechanism, involving a two-electron reduction to HO₂⁻, followed by exchange of another two electrons in the reduction of HO₂⁻ to OH⁻, has been found from the analysis of the rotating disk-ring electrode measurements viz.,:



All rate constants for this complex reaction have been determined from these measurements [148,150]. Tl and Bi adlayers cause similar catalytic effects. Tafel plots obtained from rotating disk-ring measurements show slopes of -120mV for Au/Pb and Au/Bi systems, while a slope of -55mV was found for Au/Tl. The -120mV slope, as observed for bare Au, indicates a rate-controlling first electron exchange. The slope of -55 mV was also explained by a slow first electron exchange. A low electroadsorption valency of Tl ($\alpha_{\text{Tl}} = 0.6$) had to be assumed to satisfy this slope [150].

Yeager and coworkers [147] reported interesting catalytic effects of Pb and Tl on the O₂ reduction on smooth and high surface area Pt in alkaline solutions. These effects shift the half-wave potential to more positive values than those on bare Pt (Fig. 16.16). Rotating disk-

ring electrode measurements indicate a series mechanism for O₂ reduction, instead of a direct pathway with the O-O bond scission on bare Pt.

Although Tl and Pb adsorbates on oxidized Ru surfaces in alkaline solutions differ from the UPD adlayers, their pronounced catalytic effects are noteworthy. Oxidized Ru surfaces, which are inactive for O₂ reduction, support a four-electron O₂ reduction after surface modifications upon addition of Tl⁺ and Pb²⁺ to the electrolyte [152]. Traces of Tl⁺ or Pb²⁺ were sufficient to produce catalytic effects, which were assumed to be due to a pronounced modification of the electronic properties of Ru oxides in the interaction with these cations.

16.3.5.2 Acid solutions

In acid solutions, metal adlayers on Au cause small enhancements of O₂ reduction but, except for Tl, a four-electron reduction is not observed. For Pt, a small inhibition is generally observed. A shift of 150 mV of the half wave potentials to more positive values is caused by Bi on Au(111) (Fig. 16.17), while the effect of Pb is very small [153,154]. Tl on Au(111) [155] causes a predominant four-electron reduction. O₂ reduction on silver is a four-electron reaction and is inhibited by Tl and Pb adlayers causing H₂O₂ generation as shown for Ag(111) and Ag(100) [156,153]. The inhibition was dependent on the degree of coverage and the Ag crystal plane. Catalytic effects were reported for the polycrystalline Pb/Au, Bi/Au and Tl/Au, Pb/Cu, Tl/Cu [157] and Cd/Pb [158] surfaces. Inhibition effects, however, were observed for Pt with Pb, Tl, Bi [159,157,160], Cu [159,161] and Ag [159] adlayers.

It is surprising that Pb and Cd at low coverages on Pt do not cause significant inhibition of a four-electron reduction in the kinetic control region [160,162]. This can be understood assuming a series mechanism for a four-electron reduction on Pt with adatoms. A somewhat larger inhibition was observed by Kokkinidis [157] in more concentrated solutions. These data strongly suggest that proton transfer in O₂ reduction, involving any kind of H interaction with the surface, is not likely to occur [163].

Further understanding of the catalysis of O₂ reduction by metal adlayers has been achieved by investigation of reactions on single crystal surfaces and by structure sensitive techniques. The catalytic effects observed with single crystal electrodes are in agreement with those obtained with polycrystalline surfaces [1,149]. SXS studies during the course of O₂ reduction helped to resolve the question of the coverage-dependent catalytic effect of Tl. The close-packed, rotated-hexagonal Tl phase on Au(111) was found to support predominantly two-electron reduction, while the aligned hexagonal phase in alkaline solution and patches of the (2 x 2) phase in acid solution, which gradually vanish during the reaction (see section 16.3.5), are conducive to a four-electron reduction [155].

A total inhibition of O₂ reduction on Au(111) by a Cu adlayer in the potential region where Cu forms a honeycomb ($\sqrt{3} \times \sqrt{3}$)R30° structure in the absence of O₂ was determined by STM by Itaya and coworkers [164]. Sulfate/bisulfate is adsorbed in the center of a Cu honeycomb [165,166], which could be the cause of the inhibition. A Cu submonolayer on Pt(111) causes inhibition by decreasing the current to approximately one half, while a Cu monolayer causes complete inhibition. The reduction of O₂ to H₂O₂ was assumed in the presence of either the simple or the honeycomb ($\sqrt{3} \times \sqrt{3}$)R30° submonolayer structure. A change from bridge to end-on adsorption of O₂ is viewed as a cause of the generation of

H₂O₂ and the decrease of the current by 1/2. This conclusion should be verified by RDRE measurements. A pseudomorphic Ag monolayer and a hexagonal aligned bilayer on Pt(111) cause a complete inhibition of O₂ reduction [167]. This inhibition as a function of Ag coverage was used to determine a bridge adsorption of O₂ during reduction on Pt(111).

16.3.5.3 Hydrogen peroxide reduction

H₂O₂, which is inert on most Au surfaces, except on Au(100) and its vicinals in alkaline solutions, is particularly effectively catalyzed by several Pb, Tl and Bi adlayers [1,2, 150,153]. Gewirth and coworkers [168] identified by AFM the (2 x 2)-Bi structure in the potential region at which a maximum activity for H₂O₂ reduction on Au(111) is observed. The rectangular (p x 3) Bi high coverage adlayer on Au(111) is not catalytically active for H₂O₂ reduction (Fig. 16.18), which is very similar to the inactivity of a close packed Tl adlayer on Au(111) [155]. H₂O₂ reduction is catalyzed on Au(111) with a low-coverage Tl phases, while it is almost completely suppressed by the rotated close packed hexagonal phase [169]. For the Au(111)/Pb surface, however, the highest activity was found to occur when the surface is maximally covered by Pb islands [170]. A four-electron O₂ reduction would be expected on Bi/Au(111) based on its activity for H₂O₂ reduction. This, however is not observed (cf. Fig. 16.17) and requires further attention.

16.3.5.4 Mechanisms of catalytic effects

Several mechanisms have been proposed to explain the catalytic effects of metal adlayers. These include i) specific electronic properties of the metal/adlayer surface that can increase the adsorption energy of O₂ and intermediates [1], ii) redox properties of metal

adlayers [149], and iii) formation of the bridge bond between O₂ and the Au-adatom sites, which facilitates the weakening of the O-O bond [153,169,168]. Yeager et al. [151] assumed a destabilization of anodic films on Au and Pt in the interaction with metal adlayers. McIntyre and Peck [149] proposed a redox cycle in which Tl adatoms are oxidized by O₂ and HO₂⁻ and are subsequently redeposited. Schriffrin [171] assumed a redox couple in which Pb²⁺ is oxidized by HO₂⁻ to Pb⁴⁺. Jüttner et al. [153] assumed a change from an end-on adsorption of O₂ on Au to a bridge adsorption on Au with metal adlayers. This favors the complete reduction of O₂ by weakening the O-O bond. Alvarez and Jüttner [172] reported a simulation of the catalytic effects of Pb on H₂O₂ reduction on Au(111) and Au(100) assuming essentially a lattice gas model for the Pb adlayer at low coverages and well-defined structures at high coverages. Good agreement between the simulation and experiment is considered as a support for the bridge adsorption model. However, the assumptions regarding the Pb adlayer are not in agreement with the results of SXS studies of the Pb/Au(111) system by Toney et al. [173]. Additionally, the large coverage by Pb islands, not a specific structure, was found to produce a maximum activity for H₂O₂ reduction on Au(111) [174]. No ordered structure has been reported so far for Pb on Au(100). Gewirth et al. [168] proposed a heterobimetallic bridge model for H₂O₂ interaction with the Au/Bi surface as a cause of the enhanced catalytic activity.

Ad_i_ and Wang [175] studied the UPD of Tl on Au(111) in the presence of Br⁻, which has three potential-dependent, commensurate Tl-Br phases that affect O₂ reduction in different ways (Fig. 16.19). The catalytically active (3 × 3)-2TlBr phase on Au(111) was monitored by SXS during the course of oxygen reduction by measuring the structure factors for its two low-order in-plane diffractions as a function of potential (Fig. 16.19,

insert). A decrease of their intensity ratio, $R_{0,1/1,1}$, was directly related to the rate of O_2 reduction current. Since Tl has a larger atomic form factor than Br, $R_{0,1/1,1}$ decreases as θ_{Tl}/θ_{Br} decreases (solid line). The fact that the Tl coverage decreases faster than the Br coverage with increasing O_2 reduction current suggests that the partially charged Tl adatoms undergo oxidative desorption in catalyzing the four-electron reduction of O_2 . The reaction is sustained because Tl adatoms are redeposited on the free lattice sites by the reduction of Tl^+ . Similar behavior was observed with the data for the rotated hexagonal, and hexagonal aligned Tl phases [155]. The latter phase gets easily disordered under O_2 reduction, which is not the case with the $(3 \times 3)\text{-}2TlBr$ phase because of the stabilizing effect of Br. A similar mechanism involving a redox cycle for metal adsorbates was proposed earlier [176], but the lack of clear experimental evidence has left the question of the origin of the catalytic effect open. The SXS results provide evidence for the oxidation/reduction of Tl, *i.e.*, the redox property of Tl adatoms as the origin of their catalytic effect in oxygen reduction. The observed higher activity of the low coverage Tl phases for a four-electron O_2 reduction, as opposed to that of the close packed Tl phase, can be explained with this mechanism. It appears that Tl adatoms in low coverage phases are less stable than those in close packed phases, and are consequently more active in the redox cycle described above. This mechanism should be checked with other metal adatoms and, in particular, for H_2O_2 reduction.

16.3.6 Electrodeposition of Metals

Metal adatoms have profound effects on the processes of electrodeposition of metals. The effect of the addition of trace quantities of various cations to the plating

solutions on the morphology of deposits has been known for quite some time from the plating patent literature. Usually, an increased brightness is observed in the presence of certain cations in plating solutions. In addition, catalytic effects are observed with some systems that shift the reactions to positive potentials. McIntyre and Peck [177] rationalized these observations in terms of the UPD adlayer effects with the example of the electrodeposition of Au from $\text{Au}(\text{CN})_2^-$ solutions. The adatoms of Pb and Tl induce a marked positive shift of the polarization curve and extend the current density range in which bright, fine-grained deposits are formed. It has been proposed that at sufficiently high i_M , these adatoms can act as 2D nucleation centers, with crystal growth proceeding around these centers rather than by incorporating Au atoms into the bulk lattice at the surface defects and dislocations, or by 3D growth. Davidovitch and Adami [178,179], however, have shown that Sb and Tl cause a decrease in the nucleation rate of Au deposition. The nucleation changes from instantaneous in $\text{Au}(\text{CN})_2^-$ solutions in the absence of Sb or Tl adlayers, into a progressive process in their presence (Fig. 16.20). For progressive nucleation, the rate can be described by the equation:

$$I(t) = 2 z F A N \left(\frac{2 D c}{3} \right)^{3/2} M^{1/2} t^{3/2} \quad (13)$$

where I is the current at time t , A is the area of the electrode, N is the number of nuclei that can be obtained at a given condition, and ρ is the density of the metal. As expected for progressive nucleation, the linear I versus $t^{3/2}$ plots based on eq. 13 have been obtained at constant E from the curves in Fig. 16.20b.

Sb, a well known “wetting” agent in gas phase metal deposition [180], causes remarkable morphological effects by producing very bright Au deposits at current densities at which rough deposits were obtained in its absence. Considerable catalytic

effects of Sb adatoms were ascribed to a change in the CN^- adsorption in the presence of Sb adlayers. No Sb or Tl incorporation was found with AES, or by atomic absorption spectroscopy of the dissolved deposit.

Sieradzky et al. [181, 182] have recently demonstrated that the UPD of the Pb and Cu adlayers can mediate growth of ordered multilayer deposits (up to 200 layers) of Ag on Au. Atomically flat epitaxial multilayers of Ag on Au(111) have been produced in the presence of the UPD of Pb and Cu. Ag is co-deposited with reversibly deposited UPD metal. The latter is periodically deposited and stripped from the surface, and this serves to significantly increase the density of 2D islands of Ag atoms, promoting a layer-by-layer growth mode. The UPD of the Pb monolayer covers the surface onto which the deposited Ag atoms undergo interlayer place-exchange with Pb atoms, forming 2D islands below the Pb adlayer. Upon stripping of the Pb adlayer, Ag continues to deposit with island growth. Fig. 16.21 shows a scheme of the proposed mechanism for the Pb mediated deposition of Ag on Au. An ordered multiplayer Ag deposit can also be obtained in a constant potential electrodeposition, as discussed in [176,178]. Fig. 16.22 shows the Ag deposits obtained as a function of time at a potential of 0.125 V which maintains $\theta_{\text{Pb}}=0.8$ [182].

Atomic layer control of growth is an ultimate goal of the electrodeposition of metals and nanofabrication technology, and in this context, the effects of UPD metal adlayers discussed above are very interesting. The data illustrate remarkable possibilities for further exploration of the effects of UPD adatoms in electrodeposition of metals. It would be interesting to see whether this method can produce a layer-by-layer growth in

systems with larger lattice misfits between substrate and deposit and with different chemical properties.

Acknowledgements: This research was performed under the auspices of the US Department of Energy, Divisions of Chemical and Materials Sciences, office of Basic Energy Sciences under Contract No. DE-AC02-98CH10886.

Figure captions

Fig. 16.1 Normalized Pb XANES spectra at various potentials: -0.24 V (---), 0.25 V (positive sweep) (), 0.25 V (negative sweep) (•-•-•), 0.6 V (----) and 1.15 V (••••). Reproduced with permission from reference [7].

Fig. 16.2 Current-potential curves for a mixture of pyrocatechol (1mM) and *o*-benzoquinone (1mM) on Pt and Bi/Pt rotating disk electrodes in 0.5 M HClO₄ with 1mM Bi(ClO₄)₃. Sweep rate 10 mV/s. rotation frequency (1) 12.5, (2) 25, (3) 50, (4) 75 Hz. Reproduced with permission from reference [2].

Fig. 16.3 Oxidation of HCOOH (0.26M) on Pt with Pb and Bi adlayers (full lines) and on bare Pt (dashed line) in 1 M HClO₄. Lead concentration 1mM; sweep rate 50 mV/s. Reproduced with permission from reference [34].

Fig. 16.4 Quasi-stationary current-potential plots for HCOOH (0.5 M) oxidation on sputtered Pt modified by Pb adlayer and HCOOH adsorbates in 0.1M HClO₄. Current taken 2 min after stepping the potential. The current density is given with respect to the free-Pt surface (16 % of the whole surface). Reproduced with permission from reference [36].

Fig. 16.5 Current (a) and mass signal (b,c) voltammetry curves in a 0.01 M HClO₄ solution containing 5 mM H¹²COOH: () for sputtered Pt previously with modified $\theta_{\text{Pb}}=0.36$ and $\theta_{\text{H}^{13}\text{COOH}}=0.49$; (.....) only H¹³COOH was adsorbed ($\theta_{\text{HCOOH}}=0.84$); sweep rate 100mV/s. Reproduced with permission from reference [36].

Fig. 16.6 (a) Voltammetry curve for Pt(111) with adsorbed $\theta_{\text{Bi}}=0.82(0.41)$ in 0.5 M H₂SO₄. Current multiplied by 5 for short sweep. (b) First sweep for the oxidation of 0.25 M HCOOH. Insert: Peak currents at 0.5-0.55V versus Bi coverage, (•) anodic and (×) cathodic sweeps. Reproduced with permission from reference [46].

Fig. 16.7 Comparison between experimental (\bullet) and calculated (\square) currents versus θ_{Bi} curves for the oxidation of HCOOH 0.25M on Bi/Pt(111) in 0.5M H₂SO₄ (See text for details). Reproduced with permission from reference [70].

Fig. 16.8 (a) Single potential alteration infrared (SPAIR) spectra for 0.1M HCOOH in 0.1M HClO₄ on Pt(100), and (b) Sb-modified ($\theta_{Sb}=0.25$) Pt(100), Spectra obtained during the 2mV/s anodic sweep. (c) i_{CO} (solid circles) at about 0.25 to 0.5V and peak currents (open squares) and currents at 0.35V (solid squares) versus θ_{Sb} plot. Reproduced with permission from reference [72].

Fig. 16.9 Oxidation of 1M CH₃OH in 0.5 H₂SO₄ on Pt and Pt with Sn adlayer ($\theta_{Sn}=0.34$ (0.17)). (a) current and (b) mass intensity during a potential scan of 10mV/s. Reproduced with permission from reference [102].

Fig. 16.10 (a) Voltammetry curves for the oxidation of CO on a Sn/Pt(332) surface in 0.5M H₂SO₄. $E_{ad} = 70$ mV; ($\theta_{Sn} = 0.26$ (solid line); $\theta_{Sn} = 0.03$ (dotted line); $\theta_{Sn} = 0$ (dashed line). (b) mass spectrometric responses for CO₂ generation. Reproduced with permission from reference [112].

Fig. 16.11 Current-potential curves for reduction of PhCH(NO₂)₂ (1mM) on a Pt rotating disk electrode in 0.5M HClO₄ curve (1) and Pt with adlayers of Bi, Pb and Tl, curves (2), (3) and (4), respectively. (---) Curve in base solution; concentration of cations 1 mM; sweep rate 10 mV/s; rotation frequency $f = 35$ Hz. Reproduced with permission from reference [2].

Fig. 16.12 Hydrogen evolution on a rotating Pt electrode in 1M HClO₄ in the presence of Pb adatoms. The curves 0-6 correspond to $\theta_{Pb} = 0, 0.17, 0.19, 0.56, 0.67, 0.86, 0.91$, respectively. Rotation rate 5000 rpm. Reproduced with permission from reference [132].

Fig. 16.13 H₂ evolution on a Bi/Pt(111) electrode in 0.5M H₂SO₄. Tafel plots for different Bi coverages: $\theta_{Bi} = 0, 0.13$ (0.06), 0.27(0.13), and 0.36 (0.18). Reproduced with permission from reference [137].

Fig. 16.14 (a) In-plane diffraction pattern from close packed hexagonal Tl adlayer (open circles) on Pt(111) in 0.05M H₂SO₄ solution with 1mM Tl⁺. Solid circles diffractions from Pt(111). (b) Real space model for Tl adlayer. (c) Tl-Tl interatomic distance determined from the rocking ω scans at diffraction positions as a function of potential. The electrocompression increases in solution with pH=3 beyond that observed at pH = 0, but it ceases to change when H₂ evolution starts (see text). Adapted from reference [140; reproduced with permission.

Fig. 16.15 O₂ reduction on rotating Au and Pb/Au electrodes in 1M NaOH containing 1mM HPbO₂⁻. Ring potential 0.3V, ring area 0.049cm²; sweep rate 50mV /s. Upper panel: the UPD of Pb on Au. Adapted from reference [146]; reproduced with permission.

Fig. 16.16 O_2 reduction on several substrates in 1M NaOH. Tl^+ concentrations: 3.2mM for Pt and 11mM for dispersed Pt Powecat 2000 catalyst. Pb^{2+} concentration 2mM. Sweep rate 10mV/s, for Powercat quasi steady state measurements. Electrode area 0.196 cm^2 . Pt I: no pretreatment, Pt II: cathodic pretreatment. Reproduced with permission from reference [151].

Fig. 16.17 (a) Voltammetry curve for UPD of Bi on Au in 0.5M HClO_4 containing 2mM Bi^{3+} . (b) Polarization curves for O_2 reduction on a Au rotating disk electrode (curve 1) and Bi/Au (curve 2). Sweep rate 10mV/s; $f = 16.6 \text{ Hz}$. Reproduced with permission from reference (153).

Fig. 16.18 (a) Voltammetry curve for the UPD of Bi on Au(111) in 0.1M HClO_4 solution containing 0.5mM Bi^{3+} . (b) Rotating disk polarization curve for H_2O_2 reduction in solution as in (a) with 10mM H_2O_2 . Rotation rate 400rpm; sweep rate 5mV/s. Dashed line: no Bi^{3+} . Adapted from reference [170]; reproduced with permission.

Fig. 16.19 Voltammetry curve for the UPD of Tl in 0.1M HClO_4 solution containing 1mM Tl^+ and 1mM Br^- on Au(111) (solid line) and initial parts of cathodic going sweeps for O_2 reduction on the Au(111) in the solution containing Tl^+ and Br^- (dashed line) and containing Tl^+ only (dash-dot line). Sweep rates: 20 mV/s. Structures of ordered phases are also shown, with open and shaded circles representing Br and Tl respectively. Insert: Current-potential curve obtained with O_2 reduction current (squares, left ordinate) as a function of the measured structure function intensity ratio, $R_{0,1/1,1}$, which is equal to $I_{(0,1)}/I_{(1,1)}$. The solid line shows the calculated $R_{0,1/1,1}$ (abscissa) as a function of the Tl/Br coverage ratio (right ordinate). (a) Diffraction pattern for (3×3) -2TlBr adlayer (open circles) on the Au(111) substrate (solid circles). The adlayer peaks indexed using the primitive (1.5×3) rectangular cell. Reproduced with permission from reference [175].

Fig. 16.20 (a) Potential step transients for Au deposition on Au from 0.1M Na_2SO_4 containing 50mM $\text{KAu}(\text{CN})_2$, pH=8.5; (b) Potential step transients for Au deposition on Au with Sb adlayer. Solution as in (a) with addition of 10mM Sb^{2+} . Adapted from reference [178]; reproduced with permission.

Fig. 16.21 Proposed mechanism of the UPD of Pb mediated deposition of Ag. The Ag and Pb atoms are green and gray spheres, respectively. Arrows indicate depositing metal cations. (a) Pb mediation: at potentials close to reversible Pb deposition, a Pb monolayer covers the surface. The deposited Ag adatoms undergo interlayer place-exchange with Pb adatoms (light green sphere) forming 2D islands below the Pb adlayer. (b) On the reverse cycle, the Pb adlayer is stripped from the surface as Ag continues to deposit resulting in island growth. Reproduced with permission from reference [181].

Fig. 16.22 *In situ* STM topographs showing the time evolution of the Ag layer morphology for a deposition at 0.125 V (vs. Pb/Pb^{2+}) which maintains the $\theta_{\text{Pb}} = 0.8$ in 10mM HClO_4 containing 0.1mM AgClO_4 and 10mM $\text{Pb}(\text{ClO}_4)_2$. Scan size in each image 764 x 764 nm. Reproduced with permission from reference [182].

References

- 1 R.R. Ad_i_, in *Adv. Electrochem. & Electrochem. Eng.*, vol., 13 (Ed.: H. Gerischer) J. Wiley&Sons, New York [1984), pp. 159-260.
- 2 G. Kokkinidis, *J. Electroanal. Chem.* **1986**, 201, 217-236.
- 3 A. A. Gewirth, *Chem. Rev.*, **1997**, 97, 1129-1162.
4. J. X. Wang, R.R. Ad_i_, B.M. Ocko, in *Interfacial Electrochemistry, Theory, Experiment and Applications* (Ed.: A. Wieckowski) Marcel Dekker, New York 1999, pp. 175-186.
5. K. Takayanagi, D.M. Kolb, K. Kambe, G. Lehmpfuhl, *Surf. Sci.*, **1980**, 100, 407.
6. J. T. Hupp, D. Larkin, H.Y. Liu, M.J. Weaver, *J. Electroanal. Chem.*, **1982**, 131, 229.
7. J. McBreen, M. Sansone, *J. Electroanal. Chem.*, **1994**, 373, 227-233.
8. E. Leiva, W. Schmickler, *Electrochim. Acta*, **1994**, 39, 1015-1017.
9. E. Leiva, *Surf. Sci.*, **1995**, 335, 83-90.
10. R.R. Ad_i_, A.R. Despi_, *J. Chem. Phys*, **1974**, 61, 3482-3485.
11. Z. Nagy, L.A.Curtis, N.C. Hung, D.J. Zurawski, R.M. Yonco, *J. Electroanal. Chem.*, **1992**, 325, 313-324.
12. A. Rhodes, J.M. Feliu, A. Aldaz, J. Clavilier, *J. Electroanal. Chem.*, **1989**, 271, 127-139.
13. R.R. Ad_i_, B. Z. Nikoli_, *J. Serb. Chem. Soc.*, **1992**, 57, 887-895.
14. W. Schmickler, *J. Electroanal. Chem.*, **1980**, 113, 159.
15. T. Iwasita, W. Schmickler, J.W. Schultze, *J. Electroanal. Chem.*, **1985**, 194, 355.
16. I. Fonseca, A.C. Marin, *Port. Electrochim. Acta*, **1988**, 6, 51-68.
17. G. Kokkinidis, *J. Electroanal. Chem.*, **1984**, 172, 2665.
18. A. Cappon, R. Parsons, *J. Electroanal. Chem.*, **1973**, 44, 239; **1973**, 45, 205.
19. O. Walter, J. Willsau, J. Heitbaum, *J. Electrochem. Soc.*, **1985**, 132, 1635-1638.
20. J. Willsau, J. Heitbaum, *Electrochim. Acta*, **1986**, 31, 943.
21. S.-H. Chang, L.W.H. Leung, M.J. Weaver, *J. Phys. Chem.*, **1990**, 94, 6013.
22. A. Tripkovi_, K. Popovi_, R.R. Ad_i_, *J. Chim. Phys.*, **1991**, 88, 1653.
23. B. Beden, J-M. Leger, C. Lamy, in *Modern Asp. Electrochem.* Vol. 22, [Eds.: J.O'M. Bockris, B.C. Conway, R.E. White) Plenum Press, New York, 1992, pp 97-264.
24. V.E. Kazarinov, G.Ya. Tsychnaya, V.N. Andreev, *Elektrokhimiya*, **1972**, 8, 396.
25. B. Beden, A. Bewick, K. Kunimatsu, C. Lamy, *J. Electroanal. Chem.*, **1982**, 142, 345;
26. D.S. Corigan, M.J. Weaver, *J. Electroanal. Chem.*, **1988**, 241, 143.
27. J. Clavilier, S.G. Sun, *J. Electroanal. Chem.*, **1986**, 199, 471-480.
28. R. Parsons, T. VanderNoot, *J. Electroanal. Chem.*, **1988**, 257, 9-45.
29. T.D. Jarvi, E.M. Stuve, in *Electrocatalysis*, Eds. J. Lipkowski, P.N. Ross, Wiley-VCH, New York [1998), p. 75.
30. A. Hamnett, in *Interfacial Electrochemistry*, Ed. J. Wieckowski, Marcel-Dekker, New York, [1999), p 843.
31. H. Angerstein-Kozlowska, B. MacDougall, B.E. Conway, *J. Electroanal. Chem.*, **1973**, 120, 756.
32. K.J. Cathro, *J. Electroanal. Chem.*, **1969**, 116, 1608.

-
33. M. Shibata, S. Motoo, *J. Electroanal. Chem.*, **1986**, 202, 137.
 34. R.R. Ad_i_, D.N. Simi_, A.R. Despi_, D.M. Dra_i_, *J. Electroanal. Chem.* **1975**, 65, 587-601.
 35. D. Pletcher, V. Solis, *J. Electroanal. Chem.*, **1982**, 131, 309.
 36. X.H. Xia, T. Iwasita, *J. Electrochem. Soc.*, **1993**, 140, 2559-2565.
 37. Th. Hartung, J. Willsau, J. Heitbaum, *J. Electroanal. Chem.*, **1986**, 205, 135-149.
 38. S. Ya. Vasina, R. Wetzels, L. Müller, O.A. Petrii, *Elektrokhimiya*, **1985**, 21, 413.
 39. R.R. Ad_i_, M. Podlavicky, *J. Phys.*, **1977**, 38, C5-193.
 40. R.R. Ad_i_, D.N. Simi_, A.R. Despi_, D.M. Dra_i_, *J. Electroanal. Chem.* **1977**, 80, 81-99.
 41. M.D. Spasojevi_, R.R. Adzic, A.R. Despi_, *J. Electroanal. Chem.*, **1978**, 92, 31-42.
 42. S. Motoo, M. Watanabe, *J. Electroanal. Chem.*, **1976**, 69, 429; **1979**, 98, 203.
 43. M. Shibata, O. Takahashi, S. Motoo, *J. Electroanal. Chem.*, **1988**, 249, 252-264.
 44. R.R. Ad_i_, A.V. Tripkovi_, N.M. Markovi_, *J. Electroanal. Chem.*, **1983**, 150, 79-88.
 45. T. Iwasita, X. Xia, E. Herrero, H-D. Liess, *Langmuir*, **1966**, 12, 4260-4265.
 46. J. Clavilier, A. Fernandez-Vega, J.M. Feliu, A. Aldaz, *J. Electroanal. Chem.*, **1989**, 258, 89-100; **1989**, 261, 113-125.
 47. S.-C. Chang, Y. Ho, M.J. Weaver, *Surf. Sci.*, **1992**, 265, 81-94.
 48. H-W. Kei, H. Hattori, H. Kita, *Electrochim. Acta*, **1996**, 41, 1619-1628.
 49. R.R. Ad_i_, J.X. Wang, unpublished.
 50. M.M. P. Janssen, J. Moolhuysen, *Electrochim. Acta*, **1976**, 21, 861-869.
 51. J. Clavilier, J.M. Feliu, A. Aldaz, *J. Electroanal. Chem.*, **1988**, 243, 419.
 52. U.W. Humm, D. Kramer, R.S. Zhai, D.M. Kolb, *Electrochim. Acta*, **1998**, 43, 2969-2978.
 53. J. Clavilier, J.M. Feliu, A. Aldaz, *J. Electroanal. Chem.*, **1988**, 243, 419.
 54. A. Kozawa, *J. Inorg. Chem.*, 1961, 21, 315.
 55. V.E. Kazarinov, N.A. Balashova, M.I. Kulezneva, *Elektrokhimiya*, 1965, 8, 975.
 56. R.R. Ad_i_, N.M. Markovi_, *Electrochim. Acta*, **1985**, 30, 1473.
 57. A. Fernandez-Vega, J.M. Feliu, A. Aldaz, J. Clavilier, *J. Electroanal. Chem.*, **1989**, 258, 101-113
 58. A. Fernandez-Vega, J.M. Feliu, A. Aldaz, J. Clavilier, *J. Electroanal. Chem.*, **1991**, 305, 229-240.
 59. X.H. Xia, *Electrochim. Acta*, **1999**, 45, 1057-1066.
 60. M.J. Llorca, E. Herrero, J.M. Feliu, A. Aldaz, *J. Electroanal. Chem.*, **1994**, 373, 217-225.
 61. E. Herrero, M.J. Llorca, J.M. Feliu, A. Aldaz, *J. Electroanal. Chem.*, **1995**, 394, 161-167.
 62. J. Clavilier, R. Parsons, R. Durand, C. Lamy, J.M. Leger, *J. Electroanal. Chem.*, **1981**, 124, 321.
 63. M. Zhang, C.P. Wilde, *J. Electroanal. Chem.*, **1995**, 390, 59-68.
 64. X.H. Xia, T. Iwasita, *J. Electrochem. Soc.*, **1993**, 143, 2559-2565.
 65. T. Iwasita, R. Dalbeck, E. Pastor, X. Xia, *Electrochim. Acta*, **1994**, 39, 1817-1823.
 66. J. Clavilier, *J. Electroanal. Chem.*, **1987**, 236, 87.
 67. S.-C. Chang, Y. Ho, M. J. Weaver, *Surf. Sci.*, **1992**, 265, 81-94.

-
68. C.A. Lukas, N.M. Markovi_, B.N. Grgur, P.N. Ross, *Surf. Sci.* **2000**, 448, 65-76.
C.A. Lukas, N.M. Markovi_, P.N. Ross, *Surf. Sci.* 2000, **448**, 77-86
69. S.P.E. Smith, H.D. Abru_a, *J. Electroanal. Chem.*, **1999**, 467, 43-49.
70. E. Leiva, T. Iwasita, E. Herrero, J.M. Feliu, *Langmuir*, **1997**, 13, 6287-6293.
71. J.M. Feliu, A. Fernandez-Vega, J.M. Orts, A. Aldaz, *J. Chim. Phys.*, **1991**, 88 1493-1518
72. N. Kizhakevariam, M. J. Weaver, *Surf. Sci.* **1994**, 310, 183-197.
73. S. Motto, M. Watanabe, *J. Electroanal. Chem.*, **1979**, 98, 203.
74. G.A. Attard, A. Banister, *J. Electroanal. Chem.*, **1991**, 300, 467.
75. M. Baldauf, D.M. Kolb, *J. Phys. Chem.*, **1996**, 100, 11375-11381.
76. L.A. Kilber, M. Kleinert. R. Randler, D.M. Kolb, *Surf. Sci.*, **1999**, 443, 19-30.
77. H. Naohara, S. Ye, K. Uosaki, *J. Phys. Chem. B*, **1998**, 102, 4366.
78. K. Uosaki, S. Ye, H. Naohara, Y. Oda, T. Haba, T. Kondo, *J. Phys. Chem., B* **1997**, 101, 7566.
79. E. Herrero, K. Franszczuk, A. Wieckowski, *J. Electroanal. Chem.*, **1993**, 361, 269;
W. Chrzarnowski, H. Kim, A. Wieckowski, *Catal. Lett.* **1998**, 50, 69.
80. M.J. Llorca, A.J. Feliu, A. Aldaz, J. Clavilier, *J. Electroanal. Chem.*, **1994**, 376, 151-160.
81. Yu. B. Vassilyev, V.S. Bagotzky, O.A. Khazova, *Elektrokhimiya*, **1975**, 11, 1505.
82. K. Franszczuk, E. Herrero, P. Zelenay, A. Wieckowski, J. Wang, R.I. Masel, *J. Phys. Chem.*, **1992**, 96, 8509.
83. E. Herrero, P. Zelenay, A. Wieckowski, *J. Phys. Chem.*, **1994**, 98, 5074.
84. S. Wilhelm, T. Iwasita, W. Vielstich, *J. Electroanal. Chem.*, **1987**, 238, 383-391.
85. B. Beden, F. Hahn, S. Juanto, C. Lamy, J.-M. Leger, *J. Electroanal. Chem.*, **1987**, 225, 215-225; S. Juanto, B. Beden, F. Hahn, J.-M. Leger and C. Lamy, *J. Electroanal. Chem.*, **1987**, 237, 119-129.
86. T. Iwasita, F.C. Nart, B. Lopez, W. Vielstich, *Electrochim. Acta*, **1992**, 37, 2361-2367.
87. R.J. Nichols, A. Bewick, *Electrochim. Acta*, **1988**, 33, 1691-1694.
88. H. Kita, H-W. Lei, *J. Electroanal. Chem.*, **1995**, 388, 167-177.
89. T. Iwasita, X. Xia, E. Herrero, H.-D. Liess, *Langmuir*, **1996**, 12, 4260-4265.
90. S. Srimarlu, T.D. Jarvi, E. M. Stuve, *J. Electroanal. Chem.*, **1999**, 467, 132-142.
91. Yu. B. Vassiliev, V.S. Bagotskii, N.Y. Osetrova, A.A. Mikhailova, *J. Electroanal. Chem.*, **1979**, 97, 63.
92. R.R. Ad_i_, *Israel J. Chem.*, **1979**, 18, 166-181.
93. M. Shibata, S. Motoo, *J. Electroanal. Chem.*, **1987**, 229, 385.
94. Yu. B. Vassiliev, V.S. Bagotskii, N.Y. Osetrova, A.A. Mikhailova, *J. Electroanal. Chem.*, **1979**, 97, 63
95. S. Motoo, M. Watanabe, *J. Electroanal. Chem.*, **1976**, 69, 429; M. Watanabe, S. Motoo, *J. Electroanal. Chem.*, **1975**, 60, 259,267.
96. B. Beden, F. Kadirgan, C. Lamy, J.M. Leger, *J. Electroanal. Chem.*, **1982**, 142, 171.
97. G. Kokkinidis, D. Jannakoudakis, *J. Electroanal. Chem.*, **1983**, 153, 185-200.
98. S.A. Campbell, R. Parsons, *J. Chem. Soc. Faraday Trans.*, **1992**, 88, 833-841.
99. E. Lamy-Pitara, L.El Ouazzani-Benhima, J. Barbier, M. Cahoreau, J. Caisso, *J. Electroanal. Chem.*, **1994**, 233-242.

-
100. A.N. Haner, P.M. Ross, *J. Phys. Chem.*, **1991**, 95, 3740.
 101. T. Frelink, W. Vischer, A.P. Cox, J.A.R. van Veen, *Electrochim. Acta*, **1995**, 40, 1537, -1543; T. Frelink, W. Vischer, J.A.R. van Veen, *Surf. Sci.*, **1995**, 335, 353-360.
 102. B. Bittins-Cattaneo, T. Iwasita, *J. Electroanal. Chem.*, **1987**, 238, 151.
 103. M. Shibata, N. Furuya, M. Watanabe, S. Motoo, *J. Electroanal. Chem.*, **1989**, 263, 97-102.
 104. P. Shiller, A.B. Anderson, *Surf. Sci.*, **1990**, 236, 225-232.
 105. A. Anderson, E. Grantscharova, S. Seong, *J. Electrochem. Soc.*, **1996**, 143, 2075-2082.
 106. S. Motoo, M. Watanabe, *J. Electroanal. Chem.*, **1980**, 111, 261.
 107. M. Watanabe, M. Shibata, S. Motoo, *J. Electroanal. Chem.*, **1985**, 187, 161.
 108. S.-C. Chang, M.J. Weaver, *Surf. Sci.*, **1991**, 241, 11.
 109. B. E. Hayden, A. J. Murray, R. Parsons, D. J. Pegg, *J. Electroanal. Chem.*, **1996**, 409, 51.
 110. W-F. Lin, Sog. Sun, Z-W. Tian, *J. Electroanal. Chem.*, **1994**, 364, 1-7.
 111. E. Herrero, A. Rodes, J.M. Perez, J.M. Feliu, A. Aldaz, *J. Electroanal. Chem.*, **1995**, 393, 87-96.
 112. H. Massong, S. Tillman, T. Langkau, E.A. Abd El Meguid, and H. Baltruschat, *Electrochim. Acta*, **1998**, 44, 1379-1388.
 113. P. Berenz, S. Tillmann, H. Massong, H. Baltruschat, *Electrochim. Acta*, **1998**, 43, 3035-3043.
 114. K. Wang, H.A. Gasteiger, N.M. Markovic, P.N. Ross, *Electrochim. Acta*, **1996**, 41, 2587-2593.
 115. S. Motoo, M. Shibata, *J. Electroanal. Chem.*, **1982**, 139, 119.
 116. G. Kokkinidis, D. Jannakoudakis, *J. Electroanal. Chem.*, **1982**, 133, 307.
 117. R.R. Adžić, M.S. Levata, *J. Serb. Chem. Soc.*, **1982**, 47, 83.
 118. F. Kadirgan, B. Beden, C. Lamy, *J. Electroanal. Chem.* 1983, 143, 135.
 119. K. Takamura, M. Sakamoto, *J. Electroanal. Chem.*, **1980**, 113, 273.
 120. G. Kokkinidis, J.M. Leger, C. Lamy, *J. Electroanal. Chem.*, **1988**, 242, 221.
 121. S.B. Brummer, M.J. Turner, H. Feng, *J. Appl. Electrochem.*, 1976, 6, 377.
 122. H. Druliolle, K.B. Kokoh, B. Beden, *J. Electroanal. Chem.*, 1995, 385, 77-83.
 123. G. Kokkinidis, E. Coutouli-Argilopoulou, *Electrochim. Acta*, 1985, 30, 1611; G. Kokkinidis, G. Papanastasiou, *Electrochim. Acta*, **1989**, 34, 803.
 124. C. Hasiotis, G. Kokkinidis, *Electrochim. Acta*, **1992**, 37, 1231; G. Kokkinidis, A. Papoutis, G. Papanastasiou, *J. Electroanal. Chem.*, **1993**, 359, 253.
 125. G. Kokkinidis, K. Jüttner, *Electrochim. Acta*, **1981**, 26, 971.
 126. G. Kokkinidis, K. Hasiotis, D. Sazou, *Electrochim. Acta*, **1990**, 35, 1957-1964.
 127. A. Papoutsis, G. Kokkinidis, *J. Electroanal. Chem.*, **1994**, 371, 231-239.
 128. H. Druliolle, K.B. Kokoh, B. Beden, *J. Electroanal. Chem.*, **1995**, 385, 77-83.
 129. N. Furuya, S. Motoo, *J. Electroanal. Chem.*, **1979**, 100, 771; **1982**, 139, 105.
 130. N. Furuya, S. Motoo, *J. Electroanal. Chem.*, **1976**, 72, 165-170.
 131. N. Furuya, S. Motoo, *J. Electroanal. Chem.*, **1979**, 98, 195; **1979**, 99, 19.
 132. R.R. Adžić, M.D. Spasojević, A.R. Despić, *Electrochim. Acta*, **1979**, 24, 569-576; **1979**, 24, 577-579.

-
133. J.A.M.Abd.E.-Halim, K. Jüttner, W.J. Lorenz, *J. Electroanal. Chem.*, **1979**, 106, 193.
134. E. Protopopoff, P. Marcus, *J. Chim. Phys.*, 1991, **88**, 1423-1452.
135. G.A. Martin, in *Metal-Support and Metal-Additive Effects in Catalysis*, ed. B. Imelik, C. Naccache, G. Coudurier, H. Praliaud, P. Meriaudeau, P. Galezzot, G.A. Martin, J.C. Vedrine, Elsevier, Amsterdam [1982], p. 315.
- 136 J. Clavilier, J.M. Feliu, A. Fernandez-Vega, A. Aldaz, *J. Electroanal. Chem.*, **1990**, 294, 193-208.
137. R. Gomez, A. Fernandez-Vega, J.M. Feliu, A. Aldaz, *J. Phys. Chem.*, **1993**, 97, 4769-4776; R. Gomez, J.M. Feliu, A. Aldaz, *Electrochim. Acta*, **1997**, 42, 1675-1683.
138. N. Furuya, S. Motoo, *J. Electroanal. Chem.*, **1977**, 78, 243-256.
139. L.J. Gao, B. E. Conway, *J. Electroanal. Chem.*, **1995**, 395, 261-271.
140. R.R. Ad_i_, J.X. Wang, O.M. Magnussen, B.M. Ocko, *J. Phys. Chem.*, **1996**, 100, 14721-14725.
141. D.M. Dra_i_, L. Vorkapi_, *Corrosion Sci.*, **1978**, 18, 907.
142. K. Juttner, *Werkst. Korrosion*, **1980**, 31, 358.
143. D.M. Dra_i_, V. Nakic, *29th ISE Meeting*, Budapest, 1978.
144. D.M. Dra_i_, C.S. Hao, *Corrosion Sci.*, **1983**, 23, 683.
- 5.. 148. E.B. Yeager, *Electrochim. Acta*, **1984**, 29, 1527.
146. R.R. Adzic, A. V. Tripkovic, N.M. Markovic, *J. Electroanal. Chem.*, **1980**, 114, 21; R.R. Ad_i_, A. V. Tripkovic, R. T. Anatasoski, *J. Electroanal. Chem.*, **1978**, 94, 231.
147. R. Amadelli, J. Molla, P. Bindra, E. Yeager, *J. Electrochem. Soc.*, **1981**, 128, 2706.
148. R.R. Ad_i_, N.M. Markovi_, A.V. Tripkovi_, *Bull. Soc. Chim. Belgrade*, **1980**, 45, 399.
149. J.D.E. McIntyre, W. F. Peck, Jr., in S. Bruckenstein, B. Miller, J.D.E. McIntyre, E. Yeager, Eds., *Proc. 3rd Symp. Electrode Processes*, Vol. 80-3, The Electrochem.Soc., Inc., Princeton, NJ, 1980.
150. R. Amadelli, N.M. Markovi_, R.R. Ad_i_, E. Yeager, *J. Electroanal. Chem.* **1983**, 159, 391.
151. R. Amadelli, J. Molla, E. Yeager, *J. Electroanal. Chem.*, **1981**, 126, 265.
152. N. Anastasijevi_, Z. M. Dimitrijevi_, R.R. Ad_i_, *Electrochim. Acta*, **1992**, 37, 457-464.
153. S.M. Sayed, K. Jüttner, *Electrochim. Acta*, 1983, 28, 1635.
154. K. Jüttner, *Electrochim. Acta*, **1984**, 29, 1597-1604.
155. R.R. Ad_i_, J. Wang, B.M. Ocko, *Electrochim. Acta*, **1995**, 40, 83-89.
156. A. Zwetanova, K. Jüttner, *J. Electroanal. Chem.*, **1981**, 119, 149-164.
157. G. Kokkinidis, D. Jannakoudakis, *J. Electroanal. Chem.*, **1984**, 162, 163.
158. P. Chartier, A. Sehiili, H. Nguyen Cong, *Electrochim. Acta*, **1983**, 28, 853.
159. R.R. Ad_i_, A.R. Despi_, *Z. Phys. Chem. N.F.*, **1975**, 98, 95.
160. S.A..S. Machado, A.A.Tanaka, E.R. Gonzales, *Electrochim. Acta*, **1994**, 39, 2591.
161. T. Abe, G.M. Swain, K. Sashikata K. Itaya, *J. Electroanal. Chem.* **1995**, 382, 73.
162. N. Markovi_, E. Yeager, R.R. Ad_i_, *ESM Extended Abstracts* 85:1 [1985] 919.
163. R.R. Ad_i_, in *Electrocatalysis* [Eds.: J. Lipkowski, P. Ross] Wiley-VCH Press, New York, 1998, pp.197-242.
164. T. Abe, Y. Miki, K. Itaya, *Bul. Chem. Soc. Jpn.* **1994**, 67, 2075.

-
165. Z. Shi, J. Lipkowski, *J. Electroanal. Chem.* **1994**, 365, 303.
166. M.F. Toney, J.N. Howard, J. Richer, G.L. Borges, J.G. Gordon, O.R. Melroy, *Phys. Rev. Lett.*, **1995**, 75, 4472-4475.
167. R.R. Ad_i_, J.X. Wang, *J. Phys. Chem.*, **1998**, 102, 8988-8993.
168. C-h. Chen, A.A. Gewirth, *J. Amer. Chem. Soc.*, **1992**, 114, 5439-5540; I. Oh, M.E. Biggin, A. Gewirth, *Langmuir*, **2000**, 16, 1397-1406.
169. R.R. Ad_i_, J. X. Wang, in "*Oxygen Electrochemistry*", R.R. Ad_i_, F.C. Anson, K.Kinoshita Eds., The Electrochem. Soc. Inc. Pennington, [1996], vol. 95-26 p.61.
170. C.-H. Chen, N. Washburn, A.A. Gewirth, *J. Phys. Chem.*, **1993**, 97, 9754-9760.
171. D. E. J. Schiffrin, in D. Pletcher, ed. *Electrochemistry, Specialist Periodical Reports*, vol. 8, Royal Society of Chemistry, London, 1983, p. 126.
172. M. Alvarez, K. Jüttner, *Electrochim. Acta*, **1988**, 33, 33-39.
173. M.F. Toney, J.G. Gordon, M. Samant, G.L. Borges, O.R. Melroy, *J. Phys. Chem.*, **1995**, 99, 4733-4744.
174. C.-H. Chen, N. Washburn, A.A. Gewirth, *J. Phys. Chem.*, **1993**, 97, 9754-9760.
175. R.R. Ad_i_, J.X. Wang, *J. Phys. Chem.*, **2000**, 104, 869-872.
176. McIntyre, J.D.E.; Peck, W.F., in *Proc. Third Symposium on Electrode Processes*, Bruckenstein, S.; McIntyre, J.D.E.; Miller, B.; Yeager, E.B., Eds.: The Electrochemical Society Inc.: Princeton, 1979.
177. J.D.E. McIntyre, W.F. Peck, *J. Electrochem. Soc.*, **1976**, 123, 1800.
178. Dj. Davidovi_, R.R. Ad_i_, *Electrochim. Acta*, **1988**, 33, 103-108.
179. Dj. Davidovi_, R.R. Ad_i_, *J. Serb. Chem. Soc.*, **1988**, 53, 499-510.
180. M. Copel, M.C. Reuter, E. Kaxiras, R.M. Tromp, *Phys. Rev. Lett.*, **1989**, 63, 632.
181. K. Sieradzki, S.R. Brankovi_, N. Dimitrov, *Science*, **1999**, 284, 138-141.
182. S.R. Brankovi_, N. Dimitrov, K. Sieradzki, *Electrochem. Solid State Lett.* **1999**, 2, 443-445.